Optimization Technique for Improving Torque Performance of Concentrated Winding Interior PM Synchronous Motor with Wide Speed Range

Sung-Il Kim, Ji-Hyung Bhan, and Jung-Pyo Hong
Department of Electrical Engineering
Changwon National University
Changwon, Gyeongnam, Korea
ksi1976@dreamwiz.com

Ki-Chae Lim
Electric Machine Development team / R&D Center
Dongsung Electric Machine Co., Ltd
Kimhae, Gyeongnam, Korea
dskclim@yahoo.co.kr

***Abstract*—Interior PM synchronous motors (IPMSMs) are used in many industrial and home appliance applications due to their advantages. However, the torque ripple and cogging torque of IPMSM are generally greater than those of surface permanent magnet synchronous motor. Furthermore, the IPMSM with concentrated winding is more disadvantageous than that with distributed winding in the respects. The problems are generated mainly by the discontinuous reluctance variation between the rotor and stator. Therefore, this paper proposes an optimization technique to reduce torque ripple and cogging torque without a great change of the motor parameters in the initial designed IPMSM. Moreover, the optimal models with respect to torque ripple at the base and maximum speed and cogging torque are compared with each other. In the end, response surface method combined with experimental design is applied as an optimization method, and the usefulness of the method is verified by the simulation results based on finite element analysis.**

Keywords-Experimental design; interior permanent magnet synchronous motor; optimization; response surface method

I. INTRODUCTION

Interior permanent magnet synchronous motors (IPMSMs) have many advantages such as high power density, efficiency and wide speed operation. These merits make it particularly suitable for automotive and other applications where space and energy savings are critical [1]. From the torque performance point of view, however, the IPMSM has two drawbacks. That is, torque ripple and cogging torque are relatively large as compared with a surface permanent magnet synchronous motor. In addition, the IPMSM with concentrated winding is more disadvantageous than that with distributed winding in the respects [2]. These problems are produced mostly by the discontinuous reluctance change due to the slotted structure of stator core and saturation of magnetic circuit [2], [3]. Therefore, the optimal design of IPMSM is required to improve torque performance, but it is very complex and difficult work, because not only a lot of design variables and the interactions between them must be considered but their changeable scope is wide.

In this paper, more practical and simpler optimization method is proposed to obtain improved torque performance without a great variation of the motor parameters in the initial designed IPMSM. The method is to utilize response surface method (RSM) combined with experimental design [4], [5]. The optimization procedure is divided into three parts overall. First, design variables slightly influencing the inductance and back-EMF of the initial designed IPMSM is selected. Second, their effects on torque ripple at the base and maximum speed and cogging torque are evaluated, and the design area to apply RSM is decided by experimental design and statistical analysis. Finally, in each response, the optimal shapes of IPMSM with concentrated winding are obtained by RSM. In the process, the optimal models are compared with each other, and it shows that the direction of optimal design can be changed according to the application of IPMSM. In the end, all simulation results are based on finite element analysis (FEA) and acquired in consideration of operating temperature.

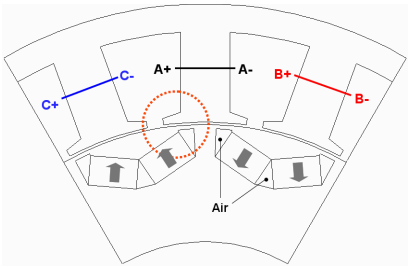

Fig. 1. Configuration of initial designed IPMSM

II. INITIAL MODEL AND ITS CHARACTERISTICS

Fig. 1 indicates the configuration of the initial designed IPMSM with concentrated winding. The constant power speed range (CPSR) of the initial model is from 680 rpm to 3400 rpm. The main dimension and specifications are listed in Table I. The characteristics of the model are calculated by FEA, voltage and torque equation, and mechanical and iron loss are ignored at that time. The equations in normal operation are expressed in d-q coordinates as follow:

$$\begin{bmatrix} v_d \\ v_q \end{bmatrix} = \begin{bmatrix} R_a & -\omega L_q \\ \omega L_d & R_a \end{bmatrix} \begin{bmatrix} i_d \\ i_q \end{bmatrix} + p \begin{bmatrix} L_d & 0 \\ 0 & L_q \end{bmatrix} \begin{bmatrix} i_d \\ i_q \end{bmatrix} \quad (1)$$

TABLE I. DEMENSION AND SPECIFICATIONS OF INITIAL DESIGNED IPMSM

Items	Value
Stator outer diameter	292 mm
Rotor outer diameter	204.8 mm
Stack length	85 mm
Air-gap	0.9 mm
Br (@120°C)	1.103 T
Number of poles	12
DC link voltage	320 V
Rated output power	20 kW
Rated current	70 A_{rms}
Base and maximum speed	680, 3400 rpm

$$T = P_n[\psi_a i_q + (L_d - L_q) i_d i_q] = P_n[\psi_a I_a \cos\beta + \frac{1}{2}(L_d - L_q) I_a^2 \sin 2\beta] \quad (2)$$

where i_d, i_q: d, q components of armature current; v_d, v_q: d, q components of terminal voltage; ψ_a: $\sqrt{3/2}\,\psi_f$; ψ_f: maximum flux linkage of permanent magnet; R_a: armature winding resistance; L_d, L_q: inductance along d-, q-axis; $p = d/dt$; P_n: number of pole pairs.

At the base and maximum speed, input armature current and current angle (β) are required to estimate accurately torque ripple by FEA. To get them, L_d and L_q must be computed according to the variation of armature current and β. In this paper, they are obtained by FEA, cubic spline interpolation and (3), and their one part is displayed in Fig. 2. In (3), ψ_a and ψ_o are fundamental components calculated from fourier analysis. The steady-state phasor diagram of IPMSM is shown in Fig. 3 [6].

$$L_d = \frac{\psi_o \cos\alpha - \psi_a}{i_d} \qquad L_q = \frac{\psi_o \sin\alpha}{i_q} \quad (3)$$

where ψ_o: total flux linkage considering the armature reaction effects; α: phase difference between ψ_a and ψ_o.

In the end, the characteristics of the initial model are predicted with L_d and L_q estimated through the way mentioned above, (1) and (2). At this time, the following limitations on armature current and terminal voltage are considered:

$$I_a = \sqrt{i_d^2 + i_q^2} \le I_{am} \quad (4)$$

$$V_a = \sqrt{v_d^2 + v_q^2} \le V_{am} \quad (5)$$

where I_{am}, V_{am}: peak values of current and voltage.

The entire torque-speed operation region considering the above control conditions is acquired in the following manner.

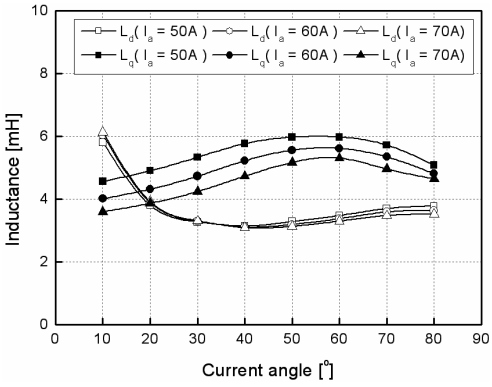

Fig. 2. L_d and L_q according to current and β

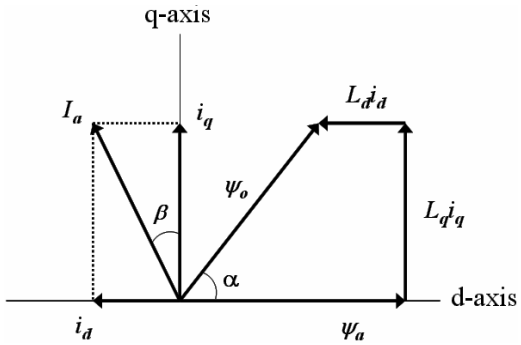

Fig. 3. Phasor diagram of IPMSM

In the anterior region of base speed, maximum torque per ampere control is employed, and flux weakening control is applied in the posterior region. As a result, Fig. 4 shows speed versus torque and output characteristic, and Fig. 5 and Fig. 6 display torque ripple at the base and maximum speed and cogging torque respectively. At that time, input current is 69 A and 63.1 A, and β is 40° and 80.6° respectively.

III. OPTIMIZATION PROCEDURE

A. Selection of Design Variables

In Section II, it is demonstrated that the performance of the initial designed IPMSM satisfies the given design conditions. In the IPMSM, the operating limits, restrictions on current and terminal voltage, and CPSR critically depend on the motor parameters such as flux linkage by permanent magnet, d- and q-axis inductance [7]. Therefore, in the initial model, the size and position of permanent magnet and air-gap length are not changed, because they greatly affect the parameters. Due to fill factor, the teeth and yoke width are not altered as well. Thus, design variables selected in this paper are barrier angle (BA), chamfer (C), slot opening (SO). Fig. 7, the magnified figure of the part surrounded a dotted line in Fig. 1, shows them and their initial dimension.

B. Use of Experimental Design

In this paper, full factorial design (FFD), one of the experimental designs, is used, and the reason is written as

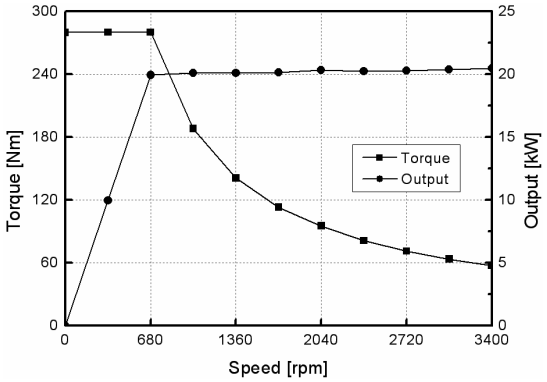

Fig. 4. Speed versus torque and output characteristic of initial model

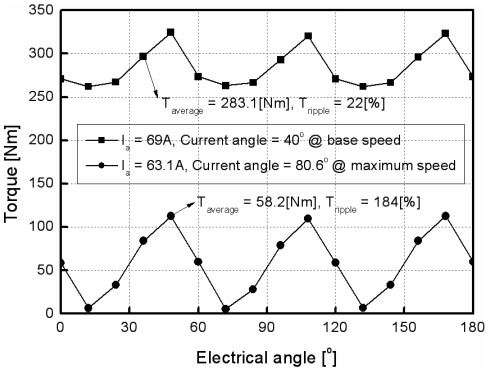

Fig. 5. Torque characteristic of initial model @ base and maximum speed

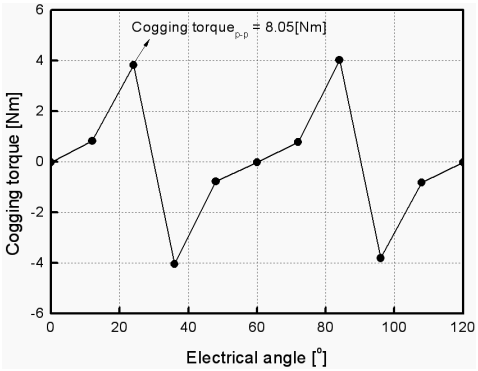

Fig. 6. Cogging torque of initial model

follows [4]. First, all combinations of the design parameters chosen in the initial model are investigated, and interaction effects between them are evaluated without confounding. Moreover, the important factors on torque ripple and cogging torque are detected by analysis-of-variance (ANOVA) [4], [5]. Second, the prediction of the responses according to the variation of the design factors is possible. Finally, the effective and reasonable design area is selected to apply RSM. In the motor design, to research the full design region needs a lot of modeling and computing time. In addition, in RSM, the accuracy of approximation greatly depends on the size of the

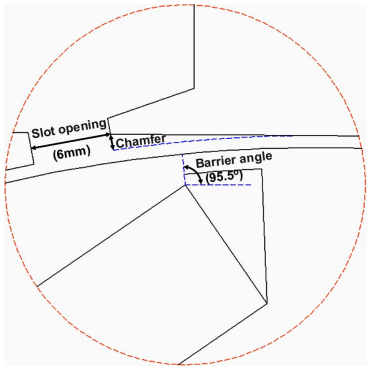

Fig. 7. Design variables and dimension of initial model

space in which the design parameters may vary [8], [9]. Accordingly, FFD is performed in the wide domain, and then RSM is applied in the best region searched by that.

Table II shows the array of 2^3 FFD to examine torque ripple and cogging torque. In the table, experiment No. 9 is added to estimate the curvature in the middle point of each design area, because it is performed at only two levels. In this paper, the levels are called "low" and "high" and denoted as "–1" and "+1" respectively. It is to convert the real value of design variable into the coded value for convenience and be calculated as follow:

$$(low, high)\ level = \frac{\zeta_i - \zeta_m}{d} \tag{6}$$

where ζ_i: the real value of each design variable; ζ_m: the mean between low and high value of each design variable; d: the difference of ζ_i and ζ_m.

The main and interaction effects of each parameter as regards torque ripple and cogging torque are shown in Fig. 8. The effects are calculated as the difference between the average responses at the low and high level of each term [4]. In Fig. 8, the factors, the most greatly influencing torque ripple at the base and maximum speed, are SO and C respectively. In the response of cogging torque, the main effect of BA and the interaction effect between BA and C, designated as BA*C in the Table II, are the most important factors. In this paper, ANOVA is used to evaluate more objectively the significance of them through statistical analysis. At that time, there is no replication of experiment. ANOVA table is shown in Table III. In the table, the sums of squares (SS) of each term and those of error and total term are given as follows:

$$SS_{term} = \frac{1}{N}\left[\begin{matrix}(total\ sum\ of\ high\ levels)\\ -(total\ sum\ of\ low\ levels)\end{matrix}\right]^2 \tag{7}$$

$$SS_E = SS_T - \left[\begin{matrix}SS_{BA} + SS_C + SS_{SO} + SS_{BA*C}\\ + SS_{BA*SO} + SS_{C*SO}\end{matrix}\right] \tag{8}$$

TABLE II. ARRAY OF 2^3 FFD AND RESULTS

Experiment No.	BA [°] (level)	C [mm] (level)	SO [mm] (level)	BA*C (level)	BA*SO (level)	C*SO (level)	Torq. ripple[%] @ base speed	Torq. ripple[%] @ max. speed	Cogging $T_{p\text{-}p}$ [Nm]
1	34.5(-1)	0.5(-1)	4(-1)	(+1)	(+1)	(+1)	22.2	108.2	0.88
2	145.5(+1)	0.5(-1)	4(-1)	(-1)	(-1)	(+1)	22.8	109.4	8.76
3	34.5(-1)	1.5(+1)	4(-1)	(-1)	(+1)	(-1)	17.6	46.0	4.44
4	145.5(+1)	1.5(+1)	4(-1)	(+1)	(-1)	(-1)	17.2	49.0	4.63
5	34.5(-1)	0.5(-1)	8(+1)	(+1)	(-1)	(-1)	8.6	79.8	1.19
6	145.5(+1)	0.5(-1)	8(+1)	(-1)	(+1)	(-1)	10.3	91.3	6.86
7	34.5(-1)	1.5(+1)	8(+1)	(-1)	(-1)	(+1)	11.2	38.6	6.56
8	145.5(+1)	1.5(+1)	8(+1)	(+1)	(+1)	(+1)	10.6	45.9	5.90
9	90(0)	1.0(0)	6(0)	(0)	(0)	(0)	14.8	90.2	1.61

TABLE III. ANALYSIS OF VARIANCE

Terms	Sum of squares(*SS*)	Degree of freedom	Mean square	F_o
BA	SS_{BA}	$\phi_{BA} = l\text{-}1$	$MS_{BA} = SS_{BA} / \phi_{BA}$	MS_{BA} / MS_E
C	SS_C	$\phi_C = m\text{-}1$	$MS_C = SS_C / \phi_C$	MS_C / MS_E
SO	SS_{SO}	$\phi_{SO} = n\text{-}1$	$MS_{SO} = SS_{SO} / \phi_{SO}$	MS_{SO} / MS_E
BA*C	SS_{BA*C}	$\phi_{BA*C} = (l\text{-}1)(m\text{-}1)$	$MS_{BA*C} = SS_{BA*C} / \phi_{BA*C}$	MS_{BA*C} / MS_E
BA*SO	SS_{BA*SO}	$\phi_{BA*SO} = (l\text{-}1)(n\text{-}1)$	$MS_{BA*SO} = SS_{BA*SO} / \phi_{BA*SO}$	MS_{BA*SO} / MS_E
C*SO	SS_{C*SO}	$\phi_{C*SO} = (m\text{-}1)(n\text{-}1)$	$MS_{C*SO} = SS_{C*SO} / \phi_{C*SO}$	MS_{C*SO} / MS_E
Error	SS_E	$\phi_E = (l\text{-}1)(m\text{-}1)(n\text{-}1)$	$MS_E = SS_E / \phi_E$	
Total	SS_T	$\phi_T = lmn\text{-}1$		

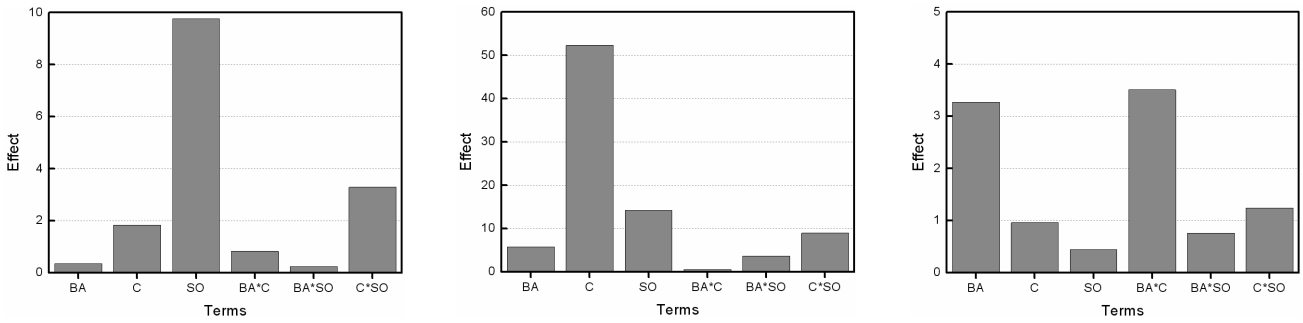

(a) Effect on torque ripple @ base speed (b) Effect on torque ripple @ maximum speed (c) Effect on cogging torque

Fig. 8. Effects on the responses of each parameter

$$SS_T = \sum_{i=1}^{lmn} y_i^{\,2} - \frac{\left(\sum_{i=1}^{lmn} y_i\right)^2}{lmn} \tag{9}$$

where N: total number of trials; y_i: *i-th* response value in the experiment; l, m and n: the number of levels in factor BA, C and SO respectively.

The ANOVA results of each response are listed in Table IV, Table V and Table VI. In the tables, the above mentioned important factors on the each response prove significant at 5% and 10% significance level respectively [4].

Fig. 9 shows the variation of each response according to main factors based on ANOVA results. In Fig. 9. (c), the interaction effect plot between BA and C is displayed, and the peak-to-peak value of cogging torque is small overall when BA is 34.5[°]. However, in the value of BA, the aspects of torque ripple at the maximum speed and cogging torque according to C occur by contraries. Therefore, in the optimal stage applied with RSM, the scope of C is the same that used in FFD.

C. *Application of RSM*

RSM is a set of statistical and mathematical techniques to find the "best fitted" response of the physical system through experiment or simulation. It has recently been recognized as an effective approach for modeling the performance of electrical devices.

TABLE IV. ANOVA OF TORQUE RIPPLE AT THE BASE SPEED

Terms	Sum of squares(*SS*)	Degree of freedom	Mean square	F_o	$F(\phi_{term}, \phi_E, 0.05)$	Significance?
BA	0.25	1	0.25	1.04	161	No
C	6.74	1	6.74	28.08	161	No
SO	190.24	1	190.24	792.67	161	Yes
BA*C	1.38	1	1.38	5.75	161	No
BA*SO	0.11	1	0.11	0.46	161	No
C*SO	21.72	1	21.72	90.5	161	No
Error	0.24	1	0.24			
Total	220.68	7				

TABLE V. ANOVA OF TORQUE RIPPLE AT THE MAXIMUM SPEED

Terms	Sum of squares(*SS*)	Degree of freedom	Mean square	F_o	$F(\phi_{term}, \phi_E, 0.05)$	Significance?
BA	66.3	1	66.3	15.35	161	No
C	5473.74	1	5473.74	1206.07	161	Yes
SO	406.31	1	406.31	94.05	161	No
BA*C	0.69	1	0.69	0.16	161	No
BA*SO	26.62	1	26.62	6.16	161	No
C*SO	161.55	1	161.55	37.4	161	No
Error	4.32	1	4.32			
Total	6139.53	7				

TABLE VI. ANOVA OF COGGING TORQUE

Terms	Sum of squares(*SS*)	Degree of freedom	Mean square	F_o	$F(\phi_{term}, \phi_E, 0.1)$	Significance?
BA	21.36	1	21.36	97.09	39.9	Yes
C	1.85	1	1.85	8.41	39.9	No
SO	0.4	1	0.4	1.82	39.9	No
BA*C	24.59	1	24.59	111.77	39.9	Yes
BA*SO	1.16	1	1.16	5.27	39.9	No
C*SO	3.09	1	3.09	14.05	39.9	No
Error	0.22	1	0.22			
Total	52.67	7				

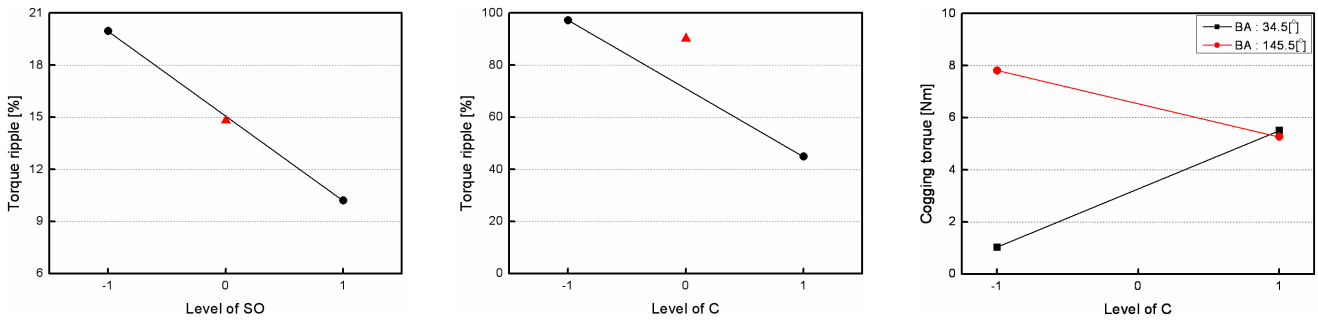

(a) Torque ripple @ base speed (b) Torque ripple @ maximum speed (c) Cogging torque

Fig. 9. Variation of responses according to main factor

In RSM, a polynomial model, called a fitted model, is generally to be constructed to represent the relationship between the performance and design parameters. Accordingly, this model provides designers with an overall prospect of the performance according to the behavior of the parameters within a design space. Nonetheless, the quality of the fitted model depends on the size of the space in which the design variables may vary. That is, as the size is small, the precision of the estimated polynomial model is higher [8]-[10]. Therefore, in this paper, FFD is applied to establish more reasonable and effective design area for RSM.

RSM is employed to make appropriate response models with respect to torque ripple and cogging torque in the initial designed IPMSM. A quadratic approximation function of the models is commonly applied to construct the fitted response surface. In general, the response model can be written as follows:

$$Y = \beta_0 + \sum_{i=1}^{k} \beta_i x_i + \sum_{i=1}^{k} \beta_{ii} x^2{}_i + \sum_{i \neq j}^{k} \beta_{ij} x_i x_j + \varepsilon \qquad (10)$$

where β is regression coefficients for design variables, ε is random error treated statistical error.

In this paper, least square method is utilized to estimate unknown coefficients, and the fitted coefficients and the fitted response model can be written as:

$$\hat{\boldsymbol{\beta}} = (\boldsymbol{X}'\mathbf{Y})^{-1} \boldsymbol{X}'\mathbf{Y} \qquad (11)$$

$$\hat{\mathbf{Y}} = \boldsymbol{X}\hat{\boldsymbol{\beta}} \qquad (12)$$

where $\boldsymbol{X}$: matrix notation of the levels of the independent variables; $\boldsymbol{X}'$: transpose of the matrix $\boldsymbol{X}$; $\mathbf{Y}$: vector of the observations.

Central composite design (CCD) is employed as the experimental design method to estimate the fitted model of each response [5]. CCD consists of three portions: a complete 2^k factorial design in which the factor levels are coded into –1 and 1; axial points at a distance α from the center point; one design center point. Table VII shows the design area of CCD based on FFD results. At that time, the width of SO is restricted to 9 mm to support coil in the slot.

From the above stated process, the polynomial models of the responses are given by (13), (14) and (15) respectively.

$$\hat{\mathbf{Y}}_{\text{Tr\_base}} = 48.4 + 0.16\text{BA} - 17.9\text{C} - 6.4\text{SO} - 0.002\text{BA}^2 + 4.1\text{C}^2 + 0.1\text{SO}^2 - 0.04\text{BA}\cdot\text{C} + 0.008\text{BA}\cdot\text{SO} + 1.7\text{C}\cdot\text{SO} \qquad (13)$$

$$\hat{\mathbf{Y}}_{\text{Tr\_max}} = 145.8 + 2.1\text{BA} - 140.5\text{C} + 7.4\text{SO} - 0.03\text{BA}^2 + 5.7\text{C}^2 - 2.6\text{SO}^2 - 0.3\text{BA}\cdot\text{C} + 0.1\text{BA}\cdot\text{SO} + 12.2\text{C}\cdot\text{SO} \qquad (14)$$

TABLE VII. DESIGN AREA BY CCD

Design factors	Levels of design factors				
	-α	-1	0	1	α
BA [°]	25.25	29	34.5	40	43.75
C [mm]	0.16	0.5	1.0	1.5	1.84
SO [mm]	5.32	6	7	8	8.68

$$\hat{\mathbf{Y}}_{\text{CT}} = -11.7 + 0.3\text{BA} - 3.8\text{C} + 2.4\text{SO} - 0.003\text{BA}^2 + 2.5\text{C}^2 - 0.1\text{SO}^2 + 0.02\text{BA}\cdot\text{C} - 0.03\text{BA}\cdot\text{SO} + 0.3\text{C}\cdot\text{SO} \qquad (15)$$

Table VIII displays the optimal conditions minimizing each response obtained by (13), (14) and (15), and Fig. 10 describes the results of each model corresponding to the point. As known in the results, the optimal points can not simultaneously minimize torque ripple at the base and maximum speed and cogging torque. Moreover, the optimal conditions of torque ripple at the maximum speed and cogging torque are located contrastively. That means the appropriate trade-off is required according to the application of IPMSM. When SO is 8.68 mm, the variation of each response is shown in Fig. 11.

IV. RESULTS AND DISCUSSION

In each optimal point, the results from the polynomial models are compared with those of FEA in Table IX. From the comparison, the models are very useful to predict the responses in the region. That is also verified by the coefficient of determination called R^2 [5], [8]. It is the statistics index to evaluate the quality of the models. R^2 of each fitted model are 0.985, 0.996 and 0.927 respectively.

TABLE VIII. OPTIMAL CONDITIONS OF EACH RESPONSE

Design factors	Optimal point @ base speed	Optimal point @ max. speed	Optimal point @ cogging torque
BA [°]	25.25	25.25	43.75
C [mm]	0.53	1.84	0.5
SO [mm]	8.68	8.68	8.68

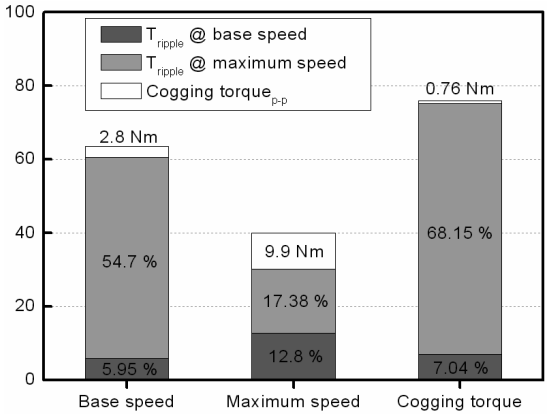

Fig. 10. Characteristic comparison of the optimal models of each response

TABLE IX. RESULT COMPARISON AT OPTIMAL POINT

Optimal model @ base speed						Optimal model @ maximum speed						Optimal model @ cogging torque					
$\hat{Y}_{Tr}$ @ base	FEA	$\hat{Y}_{Tr}$ @ max.	FEA	$\hat{Y}_{CT}$	FEA	$\hat{Y}_{Tr}$ @ base	FEA	$\hat{Y}_{Tr}$ @ max.	FEA	$\hat{Y}_{CT}$	FEA	$\hat{Y}_{Tr}$ @ base	FEA	$\hat{Y}_{Tr}$ @ max.	FEA	$\hat{Y}_{CT}$	FEA
5.95	5.62	54.7	62.3	2.8	2.86	12.8	12.4	17.4	20.7	9.9	9.6	7.0	6.9	68.2	70.7	0.76	0.8

where input current and β at the base and maximum speed are the same those of the initial designed IPMSM

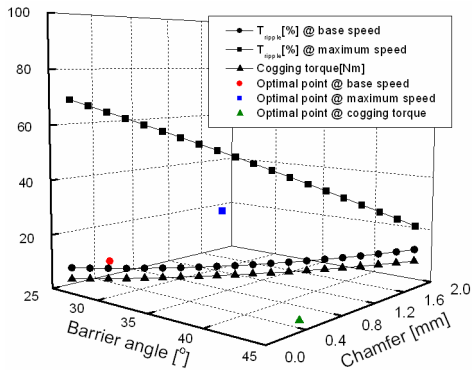

Fig. 11. Variation of each response by fitted model (SO: 8.68mm)

The torque waveform at the base and maximum speed and cogging torque of each model are shown in Fig. 12 and Fig. 13 respectively. Fig. 14 describes the average torque of the models at the base and maximum speed. In the figure, the average torque of the optimal model to minimize torque ripple at the maximum speed is the lowest of the other optimal models. The reason can be explained by (2) and the d- and q-axis inductance given in Fig. 15 and Fig. 16. That is, flux linkage (ψ_a) of the model is small as compared the other, and the fact is verified through d-axis inductance. Finally, the difference of inductance between the initial model and the model optimized at the maximum speed is relatively great. In the case, it may be impossible to guarantee CPSR as the initial model. Therefore, when the optimal design is performed, it is required to consider the ratio between flux linkage (ψ_a) and d-axis inductance as the constraint [7].

V. CONCLUSION

In this paper, RSM combined with experimental design was proposed to improve torque performance of the initial designed IPMSM with concentrated winding. With the method, the effect of the design factors as regards the torque performance of the IPMSM was evaluated, and the torque characteristics according to the variation of the parameters could be easily predicted. Moreover, it was confirmed that the focus of the optimal design according to the application of the IPMSM must be changed. In the end, the optimization technique proposed in this paper is considered as very effective design approach in optimal design of other electric machines.

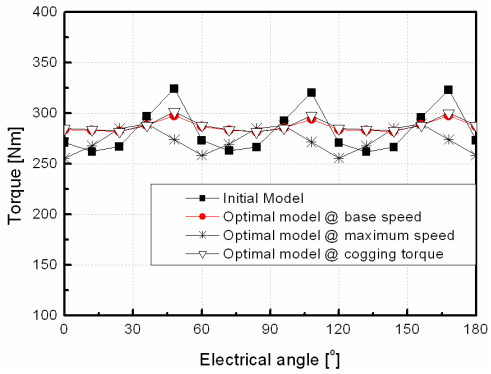

(a) @ Base speed

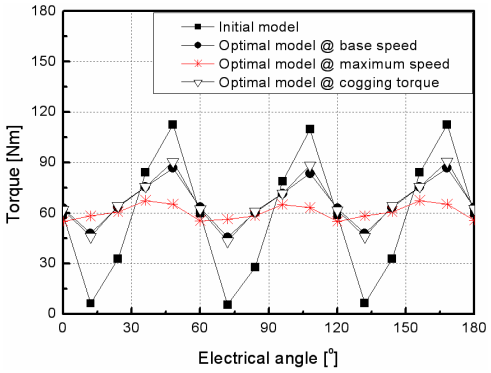

(b) @ Maximum speed

Fig. 12. Torque comparison of optimal models

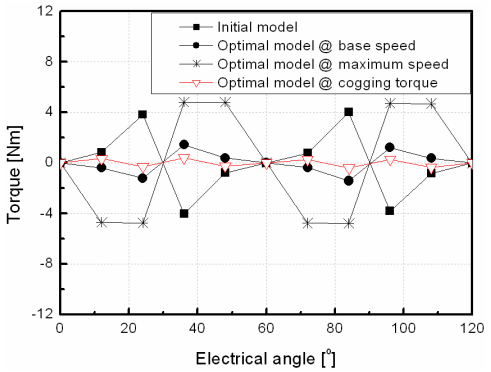

Fig. 13. Cogging torque comparison of optimal models

ACKNOWLEDGMENT

This work was supported by grant no. RTI04-01-03 from the regional technology innovation program of ministry of commerce, industry and energy (MOCIE).

REFERENCES

[1] John M. Miller, Propulsion systems for hybrid vehicles, The Institution of Electrical Engineers, 2004.

[2] Mohammad S. Islam, S. Mir, T. Sebastian, and S. Underwood, "Design consideration of sinusoidally excited permanent magnet machines for low torque ripple applications," in Conf. Rec. IEEE-IAS Annu. Meeting, 2004, CD-ROM.

[3] M. Sanada, K. Hiramoto, S. Morimoto, and Y. Takeda, "Torque ripple improvement for synchronous reluctance motor using an asymmetric flux barrier arrangement," IEEE Trans. Ind. Applicat., vol. 40, no. 4, pp. 1076-1082, July/August 2004.

[4] Douglas C. Montgomery, Design And Analysis of Experiments, John Wiley & Sons, 2001.

[5] Raymond H. Myers and Douglas C. Montgomery, *Response Surface Methodology:* Process and Product Optimization Using Design Experiments, John Wiley & Sons, 1995.

[6] S. Morimoto, Y. Takeda, and T Hirasa, "Current phase control methods for permanent magnet synchronous motors," IEEE Trans. Power Electron., vol. 5, no. 2, pp. 133-138, April 1990.

[7] S. Morimoto and Y. Takeda, "Machine parameters and performance of interior permanent magnet synchronous motors with different permanent magnet volume," Elec. Eng. in Japan , vol. 131, no. 4, pp. 1403-1408, 2000.

[8] J. T. Li, Z. J. Liu, M. A. Jabbar, and X. K. Gao, "Design optimization for cogging torque minimization using response surface methodology," IEEE Trans. Magn., vol. 40, no. 2, pp. 1176-1179, March 2004.

[9] S. Vivier, F. Gillon, and P. Brochet, "Optimization techniques derived from experimental design method and their application to the design of a brushless direct current motor," IEEE Trans. Magn., vol. 37, no. 5, pp. 3622-3626, September 2001.

[10] Y. K. Kim, Y. S. Jo, J. P. Hong, and J. Lee, "Approach to the shape optimization of racetrack type high temperature superconducting magnet using response surface methodology," Cryogenics, vol. 41, pp. 39-47, 2001.

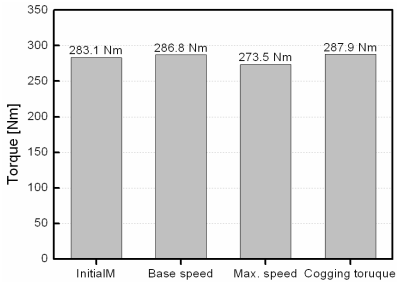

(a) @ Base speed

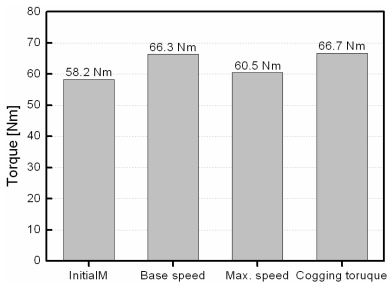

(b) @ Maximum speed

Fig. 14. Comparison of average torque

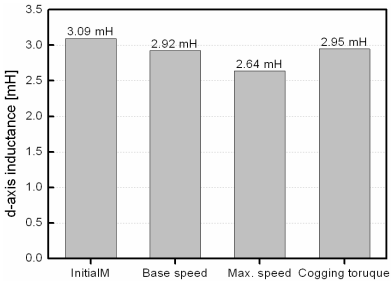

(a) d-axis inductance

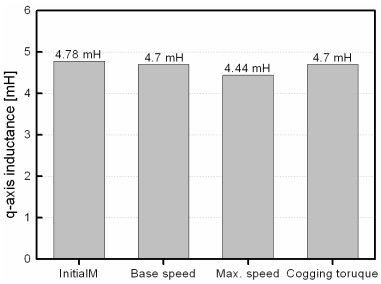

(b) q-axis inductance

Fig. 15. Comparison of inductance @ base speed

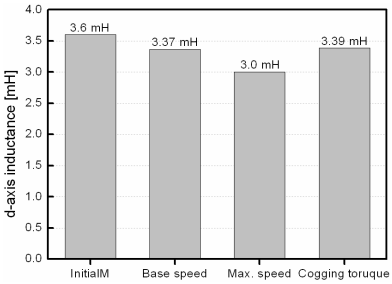

(a) d-axis inductance

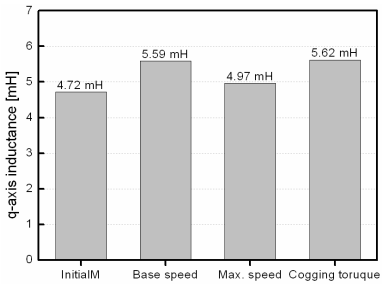

(b) q-axis inductance

Fig. 16. Comparison of inductance @ maximum speed

2006 IEEE Industry Applications Conference
Forty-first IAS Annual Meeting

GETTING STARTED
WELCOME
CONFERENCE INFORMATION
COMMITTEES
SESSIONS
AUTHORS
SEARCH

Tampa, Florida USA
8-12 October 2006

IEEE

IAS IEEE INDUSTRY APPLICATIONS SOCIETY

Papers by Session

IAS 2006

- Optimal Design for Noise Reduction in Interior Permanent Magnet Motor

  Sang-Ho Lee, Jung-Pyo Hong, Woo-Taik Lee, Sang-Moon Hwang, Ji-Young Lee and Young-Kyoun Kim

- Optimization Technique for Improving Torque Performance of Concentrated Winding Interior PM Synchronous Motor with Wide Speed Range

  Sung-Il Kim, Ji-Hyung Bhan, Jung-Pyo Hong and Ki-Chae Lim

Main Menu

Sessions

Click on title for a paper.